



MAPPING GHG EMISSION VULNERABILITY USING CONVOLUTIONAL AUTOENCODER AND MULTI-SENSOR SATELLITE IN BALI, INDONESIA

Moh Saifulloh^{1,2*}, I Gusti Ngurah Santosa³, I Nyoman Sunarta⁴, I Gusti Agung Ayu Ambarawati³, I Made Sudarma⁵, Abd. Rahman As-syakur⁵

¹Faculty of Marine Sciences and Fisheries, Udayana University, Badung, 80361, Indonesia

²Spatial Data Infrastructure Development Center (PPIDS) Denpasar City, 80225, Indonesia

³Faculty of Agriculture, Udayana University, Denpasar, 80225, Indonesia

⁴Doctoral Program of Tourism Sciences, Udayana University, 80225, Denpasar, Indonesia

⁵Research Center for Environmental (PPLH) of Udayana University, Denpasar, 80225, Indonesia

*Corresponding author: m.saifulloh@unud.ac.id

Received: April 15th 2025 / Accepted: August 7th 2025 / Published: October 1st 2025

https://doi.org/10.24057/2071-9388-2025-4005

ABSTRACT. Global warming, driven by the rising concentration of greenhouse gases (GHGs), demands innovative, datadriven approaches to assess emission vulnerability at regional scales. This study developed a novel framework utilizing an unsupervised Convolutional Autoencoder (CAE) deep learning model combined with multi-sensor satellite data to map GHG emission vulnerability. The framework integrated nine environmental indicators, including tropospheric gases, land surface temperature, vegetation cover, anthropogenic proxies, and elevation, all sourced from freely accessible remote sensing platforms. The CAE model effectively captured complex spatial patterns and reduced high-dimensional inputs into 128 latent features, enabling vulnerability assessment without requiring labeled training data. Results indicated that southern coastal regions, particularly Denpasar and Badung, exhibited the highest vulnerability due to dense urbanization and tourism-related activities. Based on zonal statistics, 11.31% of local administrative zones were identified as having high to very high vulnerability, while 18.72% were classified as moderate, and 69.97% as low to very low. The most vulnerable areas were concentrated along the southern coastline, known as a hub for tourism and economic activity, with additional pockets of vulnerability found in several northern coastal zones. These findings demonstrate the capacity of unsupervised deep learning to detect emission hotspots and spatial variability, particularly in data-limited environments. The integration of scalable algorithms with openaccess satellite data allows for rapid, cost-efficient assessments to inform evidence-based climate planning and mitigation strategies. This study introduces a practical and transferable approach for spatial quantification of GHG vulnerability, offering actionable insights for advancing global climate policy and supporting the Sustainable Development Goals.

KEYWORDS: greenhouse gas, vulnerability mapping, convolutional autoencoder, remote sensing, deep learning, spatial modeling, climate change

CITATION: Moh Saifulloh, I Gusti Ngurah Santosa, I Nyoman Sunarta, I Gusti Agung Ayu Ambarawati, I Made Sudarma, Abd. Rahman As-syakur (2025). Mapping Ghg Emission Vulnerability Using Convolutional Autoencoder And Multi-Sensor Satellite In Bali, Indonesia. Geography, Environment, Sustainability, 3 (18), 135-144 https://doi.org/10.24057/2071-9388-2025-4005

ACKNOWLEDGEMENTS: This research was conducted without financial support from any funding agency or institution. The authors gratefully acknowledge the developers of the Google Earth Engine (GEE) platform for providing open-access satellite data and tools that enabled advanced geospatial analysis. Appreciation is also extended to the open-source Python community for the development of powerful libraries used in this study. We sincerely thank the anonymous reviewers for their valuable insights and constructive feedback, which significantly improved the quality of this manuscript.

Conflict of interests: The authors reported no potential conflict of interests.

INTRODUCTION

Global climate change is widely recognized as one of the most urgent environmental challenges of the 21st century, with far-reaching implications for ecological sustainability, human health, and socio-economic development (Scafetta 2024). The primary cause of this phenomenon is the rising concentration of greenhouse gases (GHGs) in the atmosphere, which intensifies the

natural greenhouse effect and contributes significantly to global warming (Yang et al., 2022). GHGs such as carbon dioxide (CO₂), methane (CH₄), nitrogen dioxide (NO₂), and sulfur dioxide (SO₂) trap outgoing longwave radiation (Bhatti et al., 2024), thereby leading to an increase in Earth's surface temperatures (Rahaman et al., 2022). The accumulation of these gases is associated with a wide range of adverse effects, including more frequent extreme weather events, declining air quality, and disrupted

regional climate systems (Edo et al., 2024). These impacts present substantial obstacles to the achievement of the United Nations Sustainable Development Goals (SDGs), particularly Goal 13 on climate action.

Climate change, beyond its atmospheric implications, also affects the structural integrity of ecosystems and the functionality of biomes. The warming of Earth's climate alters species distributions, hydrological cycles, and ecosystem services that support agriculture, forestry, and coastal livelihoods (Dar et al., 2020; Grimm et al., 2013; Pecl et al., 2017). The majority of GHG emissions are anthropogenic, stemming from sectors such as energy, industry, transportation, agriculture, land-use change, and waste management (Priyadarshini et al., 2025). Urbanization exacerbates these emissions, with dense population centers contributing disproportionately through increased infrastructure, vehicular activity, and energy consumption. Over time, these patterns of emission become spatially correlated with zones of intense human activity and temporally aligned with rapid economic expansion (Yu et al., 2024). To address these spatial and systemic complexities, remote sensing and Geographic Information Systems (GIS) have emerged as indispensable tools for environmental analysis. Remote sensing enables continuous monitoring of Earth's surface parameters, while GIS allows for spatially explicit modeling of environmental indicators and anthropogenic pressures. These tools provide a basis for multi-scale climate vulnerability assessments, from local urban settings to regional and global contexts. For example, Valjarević et al. (2022) utilized satellite and GIS-based approaches to update global climate classification, revealing nuanced climate dynamics and spatial vulnerabilities.

Bali Province, Indonesia, a globally recognized tourism hotspot, is experiencing substantial environmental stress due to accelerated land-use transformation (Saifulloh et al., 2025). Recent research indicates that surface temperatures in Bali have been increasing at an average rate of 0.01°C per year (Sunarta et al., 2022). This trend is closely associated with the widespread conversion of natural landscapes into built environments, including hotels, resorts, restaurants, and urban settlements (Andyana et al., 2023; Diara et al., 2024; Sunarta and Saifulloh, 2022a). The loss of vegetative cover resulting from urban expansion significantly reduces the landscape's capacity for carbon sequestration (Sudarma et al., 2024; Susila et al., 2024; Trigunasih and Saifulloh, 2022), while emissions from transportation, hospitality operations, solid waste, and agricultural practices continue to intensify. Despite the significance of these transformations, there remains a lack of spatially explicit data and systematic assessments of GHG emission vulnerability for the region. This data gap highlights the need for robust geospatial methodologies to inform mitigation strategies and policy interventions.

Although various studies have sought to analyze GHG vulnerability, most have been constrained by limited spatial, temporal, or variable coverage. For instance, (Hassaan et al., 2023) assessed CO and PM2.5 exposure using discrete point-source data, lacking spatial continuity. Sakti et al. (2023) employed Sentinel-5P to monitor gaseous pollutants such as CO, NO₂, and SO₂, yet failed to incorporate critical environmental metrics such as vegetation and temperature (Pan et al., 2024). While meteorological influences have been examined in studies by (Ayyamperumal et al., 2024; Z. Feng et al., 2023), few efforts have systematically integrated these variables within spatially scalable frameworks. In the region of Bali Province, NO₂ concentrations have been examined

for the year 2020 (Sunarta and Saifulloh, 2022b), though such assessments were not embedded within a broader vulnerability framework. Meanwhile, spatial machine learning models such as fuzzy geographically weighted clustering (Grekousis et al., 2024) have incorporated static demographic indicators but still fall short of accounting for dynamic spatiotemporal GHG variability.

To overcome these limitations, the present study introduces a comprehensive approach for mapping GHG vulnerability through unsupervised deep learning. The framework employs a convolutional autoencoder (CAE), a class of neural networks capable of learning latent feature representations without requiring labeled data (Azarang et al., 2019; Cui et al., 2018). All input variables are derived from freely available multi-sensor satellite datasets, retrieved via the Google Earth Engine (GEE) platform (Gorelick et al., 2017). These include primary GHG indicators (NO₂, CO, SO₂, and Aerosol Optical Depth), environmental variables (temperature and vegetation indices), human activity proxies (population density and nighttime lights), and topographic data.

This method enables detailed spatial and temporal characterization of emission vulnerability, eliminating the need for resource-intensive field data collection. By forgoing reliance on labeled training data, the CAE model supports rapid, cost-effective, and reproducible assessments of environmental vulnerability. The innovation of this research lies in the fusion of multi-source satellite data with unsupervised deep learning to detect spatial patterns of vulnerability, particularly in data-limited regions such as Bali. Ultimately, this research advances both the scientific understanding and practical management of GHG emissions, contributing meaningfully to global climate resilience and sustainability agendas.

MATERIALS AND METHODS

Study area

The study was conducted in Bali Province, Indonesia, an island located in Southeast Asia with significant ecological sensitivity and economic reliance on tourism. Geographically, Bali lies around 8°00'S latitude and 115°40'E longitude, covering a land area of 5,593.60 km² (Fig. 1). Administratively, the province consists of nine regencies and one city: Denpasar, Badung, Gianyar, Buleleng, Tabanan, Jembrana, Klungkung, Bangli, and Karangasem, encompassing 57 subdistricts and 716 villages. According to the 2025 provincial census (BPS Bali, 2025), Bali has a population of approximately 4.46 million, with an average density of 798 people/km². Denpasar City has the highest population density (6,058 people/km²), followed by Gianyar (1,447 people/km²) and Badung (1,426 people/km²), which are the primary centers of tourism and urban development (BPS Provinsi Bali, 2025).

In terms of long-term climatic conditions, Bali experiences a tropical monsoon climate with a distinct wet and dry season. Based on historical records, average temperatures have ranged between 22.5 and 27.5°C, while projections suggest future increases to 25.5–29.5°C. Northern Bali in particular is projected to face temperature anomalies ranging from 1.6 to 2.9°C, coupled with declining humidity levels, especially in the north. In contrast, southern areas may experience slight increases in humidity. Under the representative concentration pathways (RCP) 4.5 climate scenario, Bali is predicted to lose areas with comfortable climate zones (20–26°C), giving way to predominately hot and dry conditions (Toersilowati

et al., 2022). Similarly, long-term projections suggest rainfall will fluctuate annually but remain within a relatively stable range of 2,066–2,170 mm, with both maximum and minimum temperatures continuing to rise by up to 2°C (Puspitasari and Wu, 2025). These climatic shifts pose significant implications for urban planning, agriculture, and environmental resilience in Bali, underscoring the urgent need for spatially explicit assessments of greenhouse gas vulnerability.

Workflow framework and data sources

To assess greenhouse gas (GHG) emission vulnerability spatially, a systematic methodological framework was developed, integrating multi-sensor satellite observations with unsupervised deep learning. The methodological workflow (Fig. 2) comprises three core phases: (1) data acquisition and preprocessing using Google Earth Engine (GEE), (2) deep learning modeling using a convolutional autoencoder (CAE), and (3) postprocessing and interpretation using zonal statistics.

In Phase I, remotely sensed variables were selected to reflect GHG emission sources, environmental sensitivity, and anthropogenic exposure. Table 1 outlines the nine indicators used: NO2, CO, SO2 (Sentinel-5P), NDVI, LST, AOD (MODIS), population density (WorldPop), nighttime lights (VIIRS), and elevation (SRTM). All datasets were resampled to 1 km² and reprojected to WGS 1984 UTM Zone 50S.

The open-source remote sensing data utilized in this study originated from multiple sensors with native spatial resolutions ranging from 30 meters to approximately 1,000 meters. Most of the datasets representing sources of greenhouse gas emissions, particularly from atmospheric sensors, are provided at a coarser resolution of around 1 km. Therefore, for consistency and compatibility within the modeling process, all variables were resampled to a

uniform spatial resolution of 1 km². This harmonization of spatial resolution is essential for feeding standardized input into the unsupervised deep learning model, ensuring that data dimensions are consistent (Y. Han et al., 2024; Li et al., 2024). To maintain temporal consistency across datasets, pollutant-related variables and other emission source indicators (such as NO2, CO, SO2, AOD, NDVI, and LST) were accessed using mean values coded over the 2022–2024 period via GEE. In contrast, datasets lacking temporal resolution, such as SRTM elevation and WorldPop population data, used the most recent available data. Given that this is a preliminary study conducted at a regional mapping scale, a 1 km² resolution is appropriate and consistent with similar studies implemented in other parts of the world (Garajeh et al., 2023; Maurya et al., 2022; Xiong et al., 2021).

Data preprocessing and tensor construction

Each raster file was imported using the rasterio library and converted to 32-bit floating-point arrays. Missing values were replaced with zero, particularly for elevation data beyond the study boundary. After spatial alignment, each dataset was normalized using min-max scaling to standardize feature ranges to [0, 1], following Eq. 1:

$$x_{ik}' = \frac{x_{ik} - min(x_k)}{max(x_k) - min(x_k)} \tag{1}$$

where x'_{ik} denotes the normalized value of variable k at pixel i, while min (x_k) and max (x_k) represent the minimum and maximum values observed across the entire raster for variable kk. This ensures comparability among different datasets during model training.

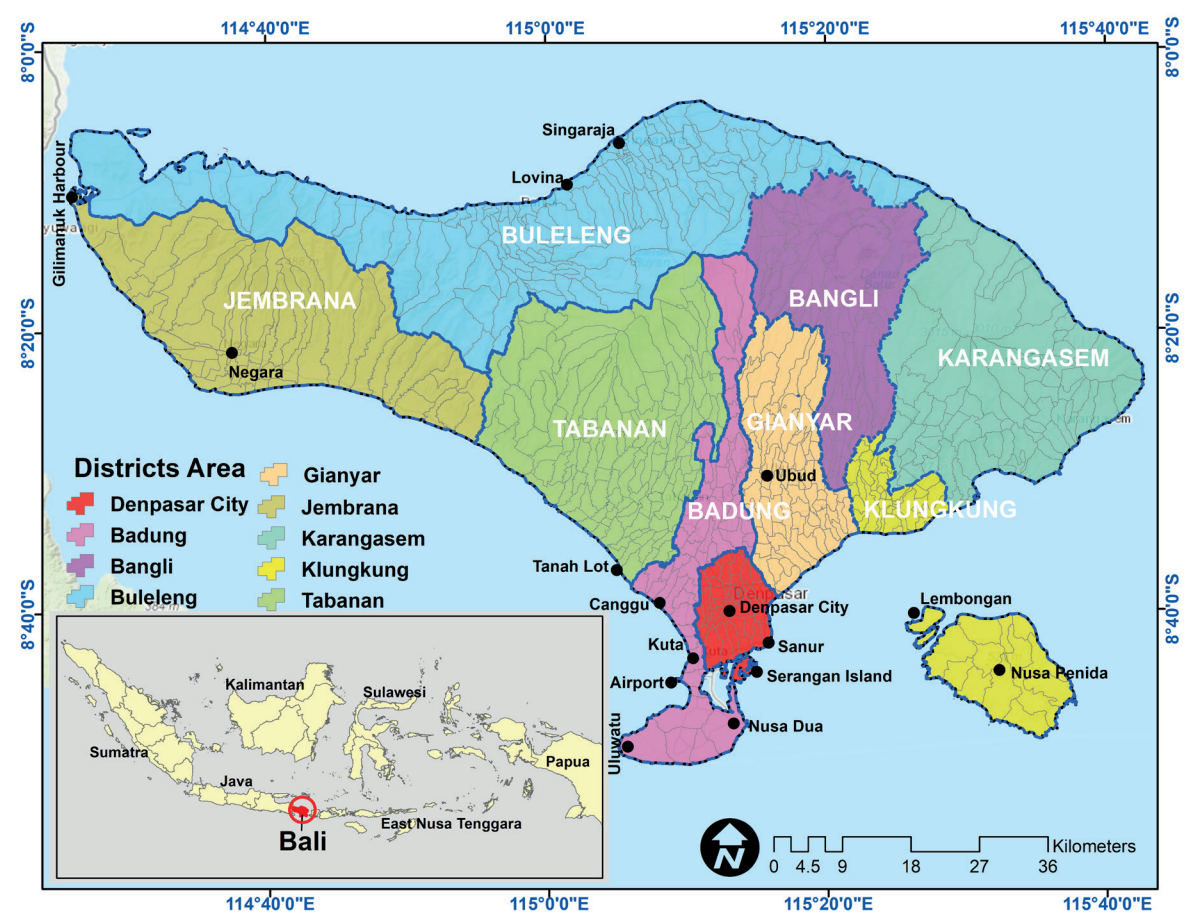


Fig. 1. Research location in Bali Province, Indonesia

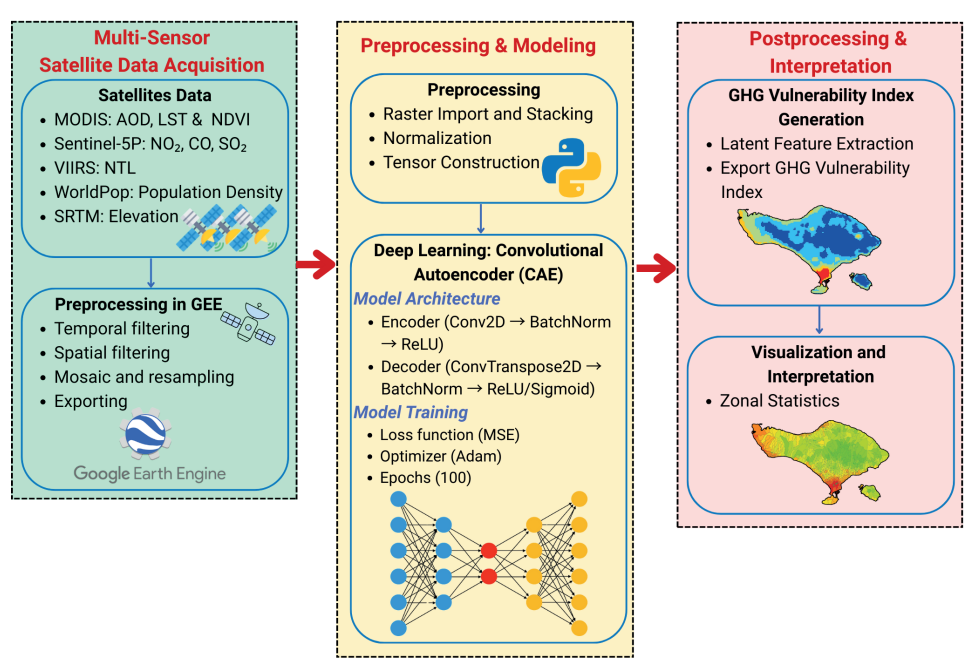


Fig. 2. Workflow Framework of the Research

Table 1. Multi-Sensor Satellite Data and Functional Roles in Regional GHG Vulnerability Modeling

Nº	Data source (GEE)	Extracted variable	Spatial & temporal resolution	Functional role in the model
1	Sentinel-5P TROPOMI (COPERNICUS/S5P/OFFL/ L3_NO2)	Tropospheric NO ₂ (mol/m²)	Pixel Size: 1113.2 meters Revisit Interval: 2 Days	Proxy for traffic and industrial emissions; indicates nitrogen- based pollution intensity
2	Sentinel-5P TROPOMI (COPERNICUS/S5P/OFFL/ L3_CO)	Tropospheric CO (mol/m²)	Pixel Size: 1113.2 meters Revisit Interval: 2 Days	Represents incomplete combustion from fossil fuel and biomass burning
3	Sentinel-5P TROPOMI (COPERNICUS/S5P/OFFL/ L3_SO2)	Tropospheric SO ₂ (mol/m²)	Pixel Size: 1113.2 meters Revisit Interval: 2 Days	Emission from power plants, volcanic activity, and smelting industries
4	MODIS MCD19A2 (MODIS/061/MCD19A2_ GRANULES)	Aerosol Optical Depth (unitless)	Pixel Size: 1000 meters Revisit Interval: Daily	Indicator of atmospheric particulate concentration; linked to PM2.5 exposure
5	MODIS Terra MOD13Q1 (MODIS/061/MOD13Q1)	NDVI (unitless)	• Pixel Size: 250 meters • Revisit Interval: 16 Days	Vegetative cover and greenness; indicator of carbon sequestration capacity
6	MODIS Terra MOD11A2 (MODIS/061/MOD11A2)	Land Surface Temperature (°C)	Pixel Size: 1000 metersRevisit Interval: 8 Days	Surface heat intensity; associated with urbanization and land energy balance
7	WorldPop 100m (WorldPop/ GP/100m/pop)	Population Density (people/ km2)	Pixel Size: 92.77 meters Revisit Interval: -	Proxy for population exposure to emissions; measures human concentration in space
8	VIIRS Nighttime Lights (NOAA/ VIIRS/DNB/MONTHLY_V1/ VCMCFG)	Nighttime Light Radiance (nW/cm2/sr)	Pixel Size: 463.83 meters Revisit Interval: Monthly	Indicator of anthropogenic energy use and urban footprint
9	SRTM DEM (USGS/ SRTMGL1_003)	Elevation (meters)	Pixel Size: 30 meters Revisit Interval: -	Terrain factor affecting air flow and pollutant accumulation in lowland areas

The normalized raster stack was reshaped into a 3D tensor $\mathcal{D} \in R^{\text{CxHxW}}$, where C is the number of channels (or features), and H and W are the spatial dimensions of the input. This tensor was further converted into a 4D tensor $X \in R^{\text{IxCxHxW}}$ to match the input format required by the convolutional autoencoder.

Convolutional autoencoder (CAE) modeling

The CAE model was implemented using the PyTorch library (Costa et al., 2024; Subramanian, 2018). It consisted

of an encoder that extracted feature representations and a decoder that reconstructed the input. The architecture was as follows.

Encoder Layers:

- Conv2D $(9 \rightarrow 32) \rightarrow BatchNorm \rightarrow ReLU$
- Conv2D (32 → 64) → BatchNorm → ReLU
- Conv2D (64 → 128) → BatchNorm → ReLU

Decoder Layers:

- ConvTranspose2D (128 → 64) → BatchNorm → ReLU
- ConvTranspose2D (64 → 32) → BatchNorm → ReLU
- ConvTranspose2D (32 → 9) → Sigmoid

The model was trained using the Mean Squared Error (MSE) loss function, defined by Eq. 2:

$$\mathcal{L}_{MSE} = \frac{1}{n} \sum_{i=1}^{n} \left(x_i - \hat{x}_i \right)^2$$
 (2)

where $x_{i,i}$ denotes the original input tensor value at index i, and \tilde{X}_i is the corresponding reconstructed output. The loss function penalizes reconstruction errors, thereby guiding the encoder to learn compact yet informative representations. The Adam optimizer was employed with a learning rate of 0.001 over 100 training epochs.

GHG vulnerability index

Upon convergence, the encoder output was extracted as a latent tensor $Z \in R^{128xHxW}$, where 128 is the number of abstract feature channels. To collapse this multidimensional feature space into a single-band vulnerability index, mean pooling was applied across all channels (Eq. 3):

$$GHG_{index} = \frac{1}{128} \sum_{c=1}^{128} Z_c$$
 (3)

where GHG_{index} is the final greenhouse gas emission vulnerability index, and Z_c is the activation of the c^{th} feature channel. The resulting index was again normalized to the range [0, 1] to facilitate interpretation. Higher index values indicate areas with a greater confluence of emission-related stressors and limited ecological buffering.

For policy-oriented interpretation, the vulnerability index raster was intersected with Bali's district-level administrative boundaries. The average vulnerability score for each administrative unit mm was calculated as Eq. 4:

$$V_m = \frac{1}{|Z_m|} \sum_{i \in Z_m} v_i \tag{4}$$

where V_m represents the mean vulnerability index of zone m, calculated by summing all pixel-level vulnerability values v_i within the set of spatial units Z_m , and dividing the result by the total number of pixels $|Z_m|$ within that zone. This procedure translated fine-resolution pixel values into actionable administrative-level metrics that can guide localized climate mitigation planning, land use policy, and emission reduction initiatives.

RESULTS

Dataset from Multi-Sensor Satellite

This study utilized nine environmental variables derived from freely available multi-sensor satellite products. These included tropospheric gases (NO₂, CO, SO₂), Aerosol Optical Depth (AOD), Land Surface Temperature (LST), vegetation indices (NDVI), anthropogenic proxies (Nighttime Light Radiance and Population Density), and Elevation (Fig. 3). All raster datasets were resampled to a uniform spatial resolution of 1 km2 and aligned to the WGS 1984 UTM Zone 50S coordinate system. Each variable was normalized to a [0,1] scale to ensure consistent input for the convolutional model.

Elevated values of NO₂, CO, SO₂, and AOD were predominantly observed in lowland urban regions. These concentrations reflect intense combustion activity and atmospheric pollutant accumulation from transportation and industrial sources. Such hotspots were spatially clustered in urban centers and along coastal corridors characterized by dense infrastructure and minimal vegetative cover. Other variables, such as LST, NDVI, population density, and nighttime lights, mirrored patterns of urban expansion. Built-up zones displayed higher land surface temperatures and lower vegetation greenness. Population and light radiance levels further emphasized anthropogenic pressure, while elevation helped determine pollutant dispersion across terrain gradients.

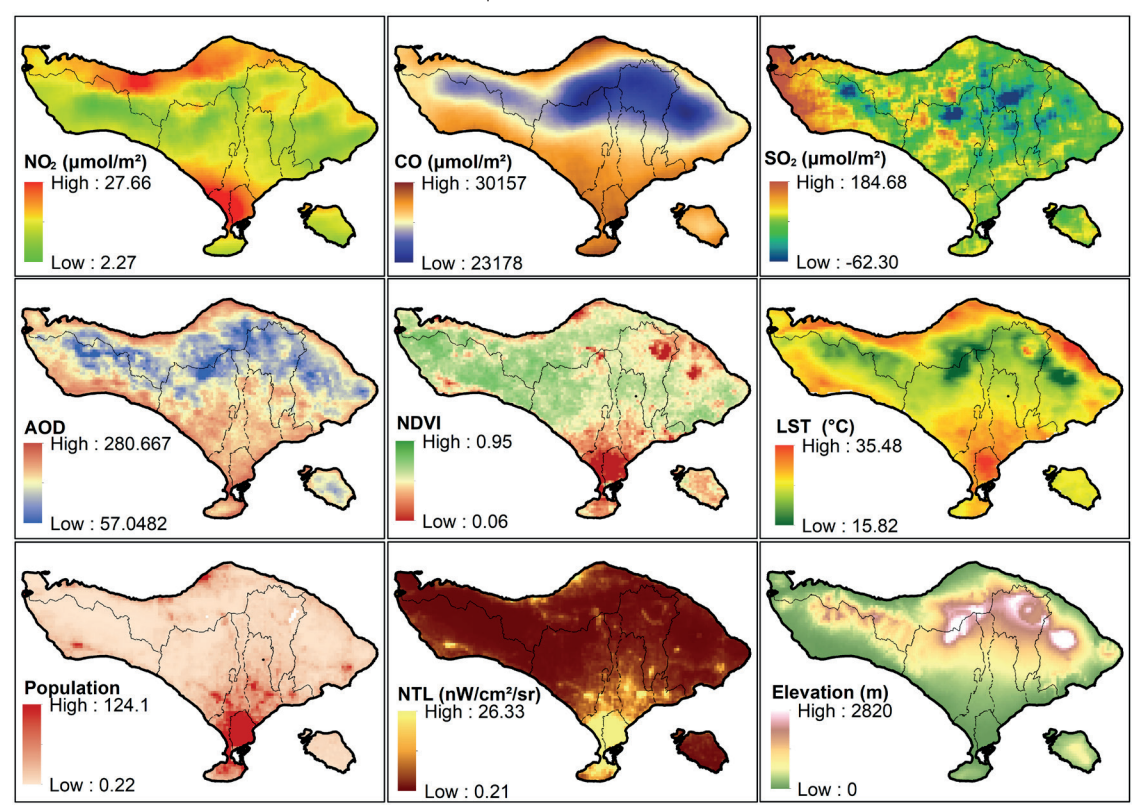


Fig. 3. Environmental variables derived from multi-sensor satellite datasets used in greenhouse gas emission vulnerability modeling

Multivariate Relationships and Feature Space Analysis

The correlation matrix (Fig. 4) identified strong associations among several variables. AOD exhibited high correlation with CO (r = 0.98), NDVI (r = 0.93), and LST (r = 0.92), indicating that areas with higher particulate concentrations often coincide with vegetation decline and thermal stress. NO $_{\rm 2}$ also showed strong correlations with CO (r = 0.92) and LST (r = 0.88). Additionally, nighttime light radiance and population density were closely linked (r = 0.89), reinforcing their combined role as indicators of urbanization intensity.

Autoencoder Training and Latent Representation

The convolutional autoencoder was trained for 100 epochs using the Adam optimizer with a learning rate of 0.001. Training loss, calculated using mean squared error (MSE), decreased from 0.195 to 0.0021 (Fig. 5), confirming effective convergence. The encoder architecture featured three convolutional layers integrated with batch normalization and ReLU activations, compressing the nine-band input into 128 latent features. The decoder then reconstructed the input using transposed convolutional layers and activation functions.

The latent feature space effectively captured non-linear dependencies among input variables, enabling the model to identify complex spatial patterns of vulnerability. For example, locations with elevated LST, high NO2, and low NDVI were consistently abstracted into high-risk zones. The low reconstruction error confirmed the model's capability to retain meaningful spatial representations. A single-band vulnerability index was generated via mean pooling across all latent feature channels.

The GHG vulnerability index was classified using the Jenks Natural Breaks method, which separates values into statistically distinct classes by minimizing withinclass variance and maximizing variance between classes. This method is widely recognized for its suitability in environmental vulnerability assessments (Hou et al., 2022; Ke et al., 2023; Rzasa and Ciski, 2021). The spatial distribution (Fig. 6) showed that very high vulnerability zones were concentrated in southern Bali, particularly in Denpasar and coastal Badung, where index values exceeded 0.66. These areas exhibited characteristics such as dense urbanization, extensive infrastructure, low vegetation cover, and intensified human activity. High vulnerability also appeared in segments of southern Gianyar and Klungkung. Moderate vulnerability values were observed in transitional inland regions, while low to very low vulnerability was dominant in upland and northern areas with greater ecological stability.

Further analysis of administrative-level units revealed that 11.31% were categorized as high or very high vulnerability, 18.72% as moderate, and 69.97% as low to very low (Fig. 7). These village-level areas represent local jurisdictions responsible for implementing environmental policy. The highest vulnerability scores were recorded in Denpasar, southern Badung, Gilimanuk (Jembrana), and Singaraja (Buleleng), all of which are recognized for concentrated tourism and urban development.

DISCUSSION

This study presents a significant advancement in spatial modeling of greenhouse gas (GHG) emission vulnerability by integrating a convolutional autoencoder (CAE) deep learning approach with multi-sensor satellite

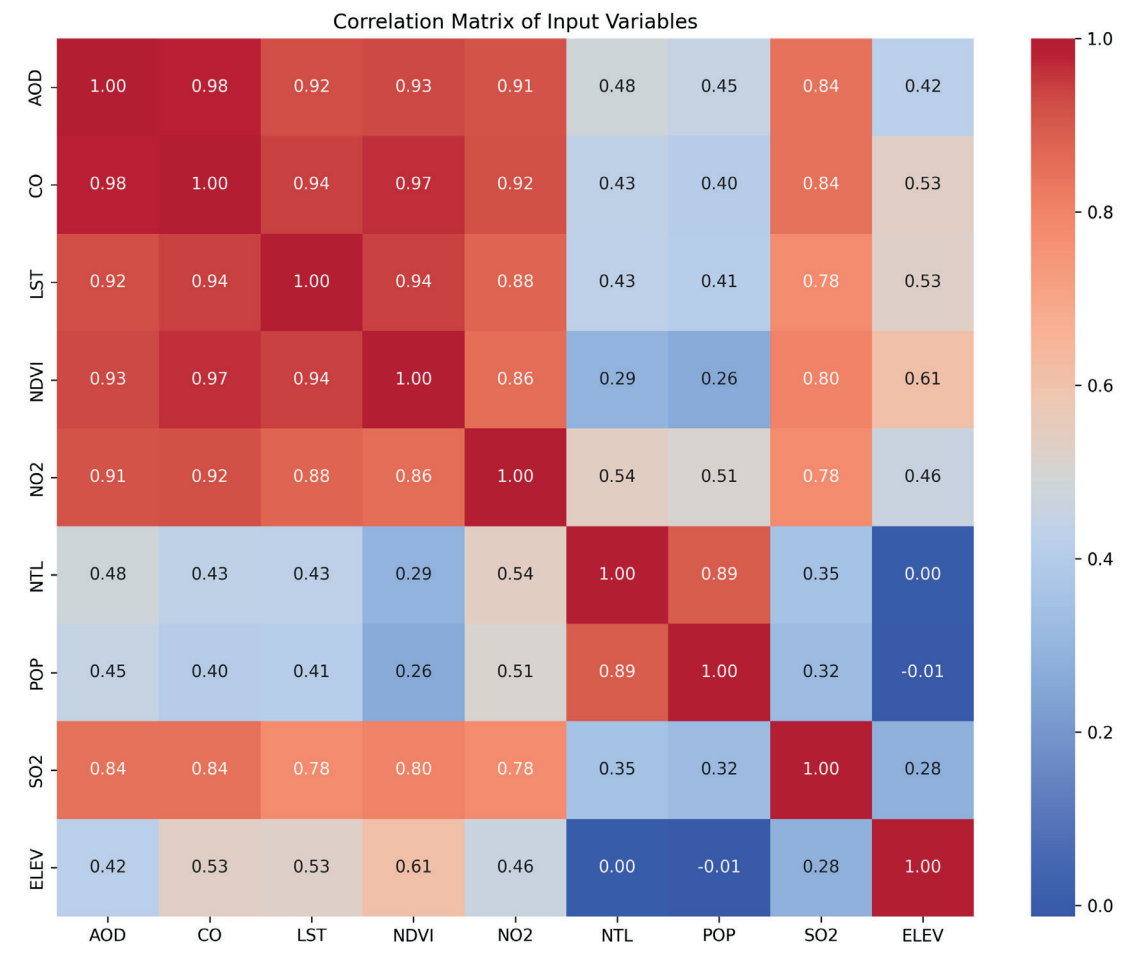


Fig. 4. Correlation matrix of environmental variables used in GHG vulnerability modeling

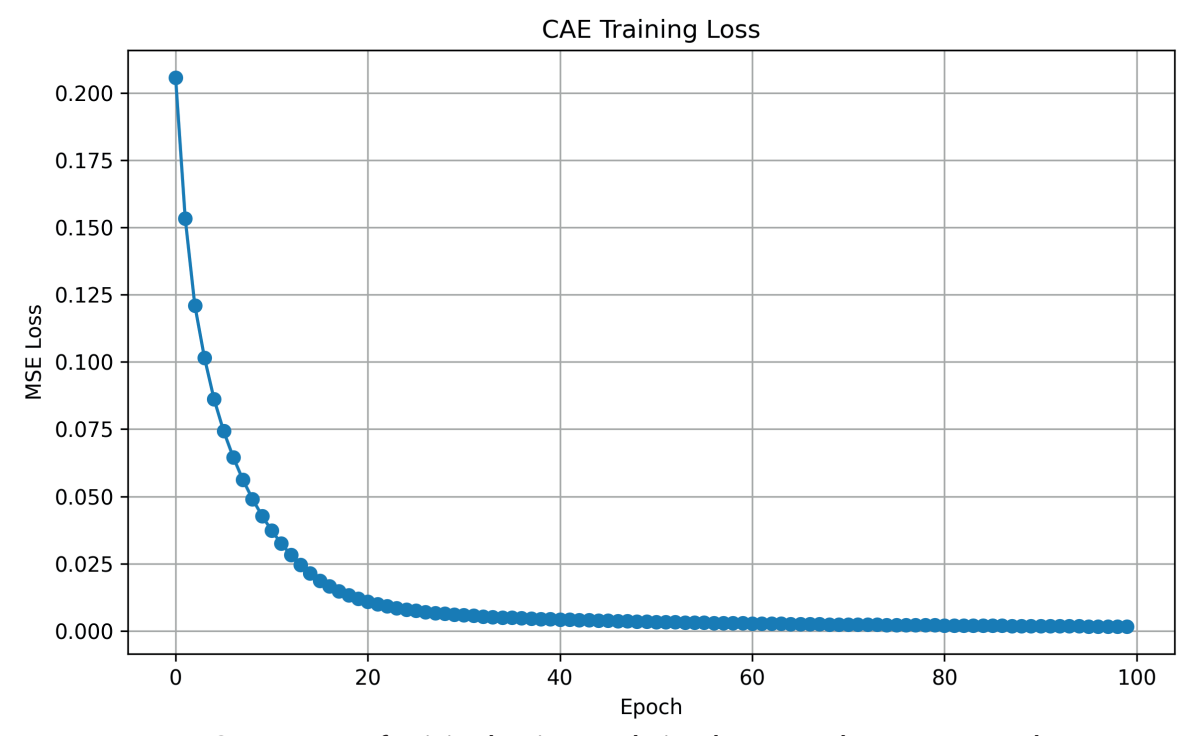


Fig. 5. Convergence of training loss in convolutional autoencoder over 100 epochs

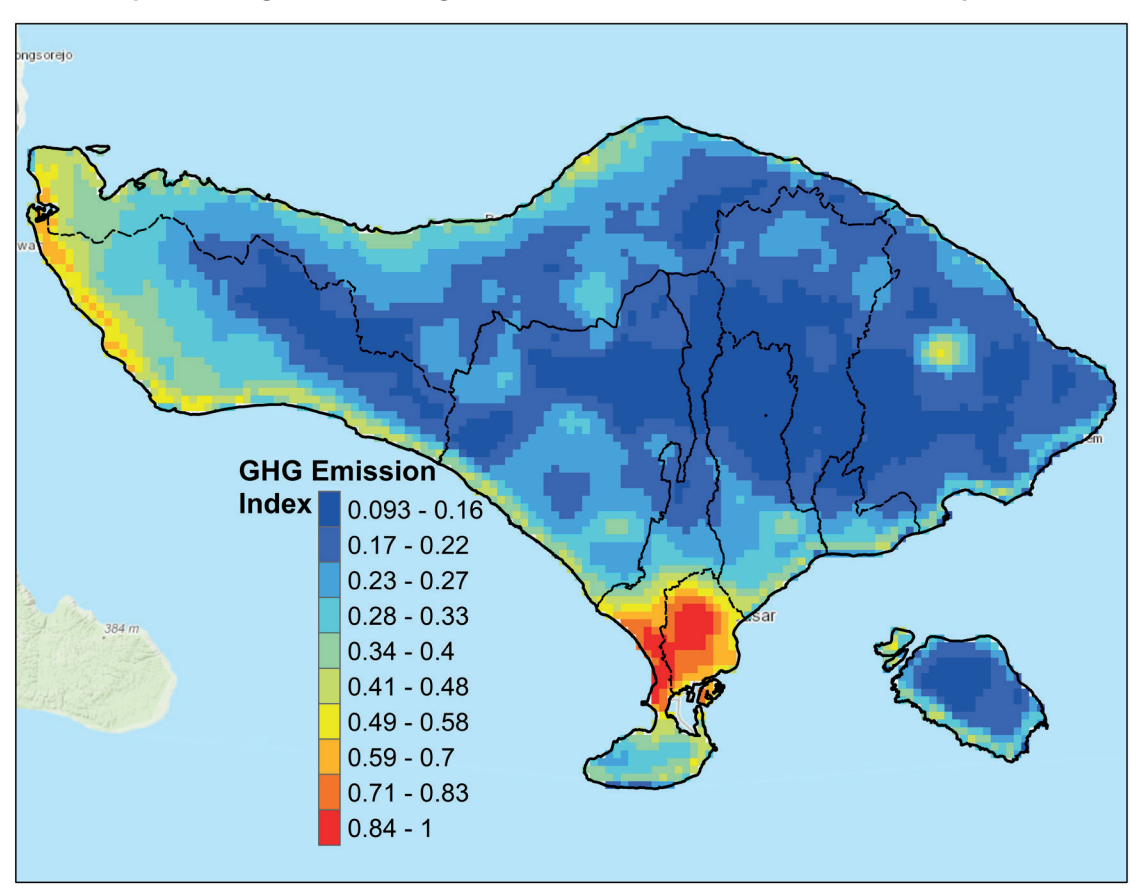


Fig. 6. Spatial distribution and proportional area of GHG emission vulnerability in Bali Province

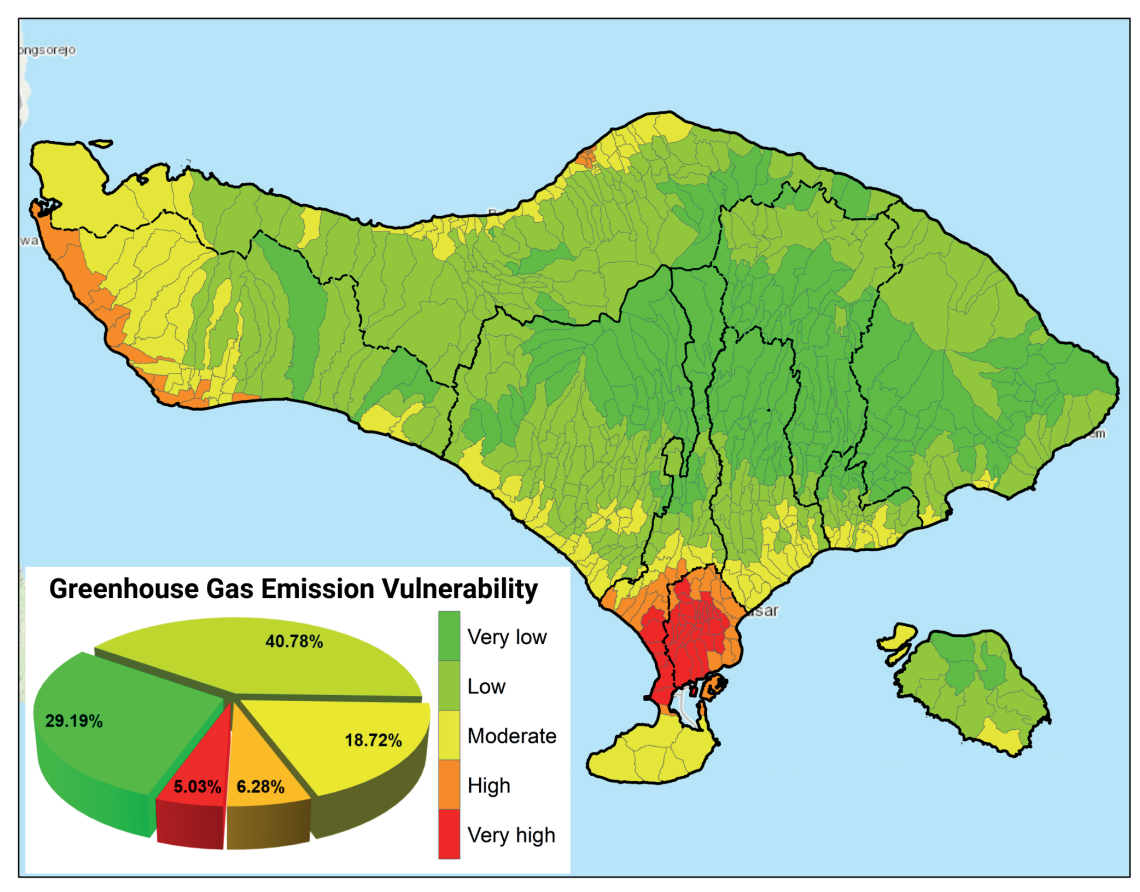


Fig. 7. Spatial alignment of GHG vulnerability with administrative boundaries

data. The unsupervised CAE model eliminated the need for labeled training data, addressing a persistent challenge in regional-scale environmental assessments where ground-based measurements are often unavailable. Previous research has demonstrated that autoencoders are effective for extracting latent features and reconstructing complex geospatial patterns in remote sensing applications (X. Han et al., 2017; Pintelas et al., 2021). In this study, the model achieved rapid convergence and low reconstruction loss, affirming its ability to process and learn from high-dimensional environmental inputs.

The resulting vulnerability index revealed distinct spatial gradients, with high-risk zones concentrated in southern coastal areas, such as Denpasar and southern Badung. These regions are associated with dense urbanization, tourism-related development, and intensive energy use. These findings align with global studies showing that atmospheric pollutants like NO₂, CO, and AOD are often concentrated in urban-industrial zones (Fioletov et al., 2025; Wang et al., 2025). The integration of land surface temperature, NDVI, nighttime lights, and population density further substantiated the mapping of anthropogenic stressors and ecological degradation (Liu et al., 2015; McRoberts et al., 2020).

A key innovation of this research is its use of openly accessible satellite data and an unsupervised deep learning approach to generate a replicable and cost-effective GHG vulnerability mapping framework. Designed to be compatible with Google Earth Engine and other open-source platforms, this methodology can be scaled to other regions lacking the technical capacity or financial means for traditional emissions monitoring. This approach complements previous efforts in urban classification and land use mapping, where autoencoder-based models have demonstrated effective generalization across geographic contexts (Jiang, 2018). The framework provides critical support for environmental planning and is aligned with the objectives of SDG 13 on climate action.

This study also acknowledges certain methodological constraints. The use of 1 km² spatial resolution, while adequate for regional-scale visualization, may not capture the fine-scale variability needed for local urban or zoning applications. Additionally, while MODIS and Sentinel-5P data offer global consistency, they may lack sensitivity to site-specific emission patterns or infrastructure dynamics. To enhance spatial detail and accuracy, future research should incorporate higher-resolution datasets such as Sentinel-1 and Sentinel-2 imagery. Furthermore, integrating thematic variables like road networks, industrial zones, localized greenhouse gas emissions inventories, and spatially distributed land use categories would provide a more comprehensive picture of emissions at finer scales (Q. Feng et al., 2021). Additional consideration should be given to incorporating landscape circulatory factors and pollutant dispersion mechanisms using digital elevation models and meteorological data that capture prevailing wind directions. The findings validate the effectiveness of combining unsupervised deep learning with multisensor remote sensing for emission vulnerability mapping. The proposed framework is transferable, cost-efficient, and capable of identifying high-risk areas, particularly in urbanizing regions. This method serves as a valuable tool for supporting spatially informed climate mitigation strategies and advancing global climate governance.

CONCLUSIONS

This study demonstrated a rapid and cost-effective approach to mapping greenhouse gas (GHG) emission vulnerability by integrating multi-sensor satellite data with an unsupervised convolutional autoencoder (CAE) deep learning model. The framework avoided the need for field-based training data and extracted 128 latent features from a range of environmental indicators, enabling robust spatial characterization of emission risks. The vulnerability

index showed distinct spatial gradients, with the highest values concentrated in southern coastal areas experiencing dense anthropogenic activity, particularly from tourism and urbanization. These results confirm the effectiveness of unsupervised deep learning in identifying emission hotspots and spatial variability in data-limited settings. Utilizing open-access datasets and scalable computational methods, the framework offers a replicable solution for other regions, especially in developing countries where financial and technical constraints hinder regular monitoring. It presents a practical tool to support emission

analysis and planning aligned with climate mitigation strategies. To enhance precision, future improvements should incorporate high-resolution imagery through data fusion techniques, such as integrating Sentinel-2 or commercial satellite data. This advancement would allow for more detailed mapping suitable for urbanscale planning and targeted mitigation. This research contributes a transferable, efficient methodology for spatial quantification of GHG emission vulnerability, offering actionable insights to support climate policy and advance the Sustainable Development Goals (SDGs).

REFERENCES

Andyana I.W.S., As-Syakur A.R., Sunarta I.N., Suyarto R., Diara I.W., Susila K.D., Saifulloh M., Kusmiyarti T.B. and Wiyanti W. (2023). Urban tourism expansion monitoring by remote sensing and random forest. IOP Conference Series: Earth and Environmental Science, 1180(1). DOI: 10.1088/1755-1315/1180/1/012046

Ayyamperumal R., Banerjee A., Zhang Z., Nazir N., Li F., Zhang C. and Huang X. (2024). Quantifying climate variation and associated regional air pollution in southern India using Google Earth Engine. Science of the Total Environment, 909. DOI: 10.1016/j.scitotenv.2023.168470

Azarang A., Manoochehri H.E. and Kehtarnavaz N. (2019). Convolutional Autoencoder-Based Multispectral Image Fusion. IEEE Access, 7. DOI: 10.1109/ACCESS.2019.2905511

Bhatti U.A., Bhatti M.A., Tang H., Syam M.S., Awwad E.M., Sharaf M. and Ghadi Y.Y. (2024). Global production patterns: Understanding the relationship between greenhouse gas emissions, agriculture greening and climate variability. Environmental Research, 245. DOI: 10.1016/j. envres.2023.118049

Costa N., Pérez L. and Sánchez L. (2024). Rapidae: A python library for creation, experimentation, and benchmarking of autoencoder models. 2024 IEEE International Conference on Fuzzy Systems (FUZZ-IEEE), 1–8.

Cui W., Zhou Q. and Zheng Z. (2018). Application of a Hybrid model based on a convolutional auto-encoder and convolutional neural network in object-oriented remote sensing classification. Algorithms, 11(1). DOI: 10.3390/a11010009

Dar J.A., Subashree K., Bhat N.A., Sundarapandian S., Xu M., Saikia P., Kumar A., Kumar A., Khare P.K. and Khan M.L. (2020). Role of major forest biomes in climate change mitigation: An eco-biological perspective. In: Environmental Science and Engineering. DOI: 10.1007/978-3-030-32463-6_24

Diara I.W., Susila K.D., Wiyanti W., Sunarta I.N., Kusmiyarti T.B. and Saifulloh M. (2024). Exploring the Influence of Various Land Use Land Cover on Land Surface Temperature of Coastal Tourism Areas in Bali Using Landsat 9. Environmental Research, Engineering and Management, 80(2), 118–132.

Edo G.I., Itoje-akpokiniovo L.O., Obasohan P., Ikpekoro V.O., Samuel P.O., Jikah A.N., Nosu L.C., Ekokotu H.A., Ugbune U. and Oghroro E.E.A. (2024). Impact of environmental pollution from human activities on water, air quality and climate change. Ecological Frontiers.

Feng Q., Niu B., Chen B., Ren Y., Zhu D., Yang J., Liu J., Ou C. and Li B. (2021). Mapping of plastic greenhouses and mulching films from very high resolution remote sensing imagery based on a dilated and non-local convolutional neural network. International Journal of Applied Earth Observation and Geoinformation, 102. DOI: 10.1016/j.jag.2021.102441

Feng Z., Wang X., Yuan J., Zhang Y. and Yu M. (2023). Changes in air pollution, land surface temperature, and urban heat islands during the COVID-19 lockdown in three Chinese urban agglomerations. Science of the Total Environment, 892. DOI: 10.1016/j.scitotenv.2023.164496 Fioletov V., McLinden C.A., Griffin D., Zhao X. and Eskes H. (2025). Global seasonal urban, industrial, and background NO2 estimated from TROPOMI satellite observations. Atmospheric Chemistry and Physics, 25(1), 575–596.

Garajeh K.M., Laneve G., Rezaei H., Sadeghnejad M., Mohamadzadeh N. and Salmani B. (2023). Monitoring Trends of CO, NO₂, SO₂, and O3 Pollutants Using Time-Series Sentinel-5 Images Based on Google Earth Engine. Pollutants, 3(2). DOI: 10.3390/pollutants3020019

Gorelick N., Hancher M., Dixon M., Ilyushchenko S., Thau D. and Moore R. (2017). Google Earth Engine: Planetary-scale geospatial analysis for everyone. Remote Sensing of Environment, 202. DOI: 10.1016/j.rse.2017.06.031

Grékousis G., Sunarta I.N. and Stratoulias D. (2024). Tracing vulnérable communities to ambient air pollution exposure: A geodemographic and remote sensing approach. Environmental Research, 258, 119491.

Grimm N.B., Chapin F.S., Bierwagen B., Gonzalez P., Groffman P.M., Luo Y., Melton F., Nadelhoffer K., Pairis A., Raymond P.A., Schimel J. and Williamson C.E. (2013). The impacts of climate change on ecosystem structure and function. In: Frontiers in Ecology and the Environment, Vol. 11, Issue 9. DOI: 10.1890/120282

Han X., Zhong Y. and Zhang L. (2017). Spatial-spectral unsupervised convolutional sparse auto-encoder classifier for hyperspectral imagery. Photogrammetric Engineering and Remote Sensing, 83(3). DOI: 10.14358/PERS.83.3.195

Han Y., Chi H., Huang J., Gao X., Zhang Z. and Ling F. (2024). TemPanSharpening: A multi-temporal Pansharpening solution based on deep learning and edge extraction. ISPRS Journal of Photogrammetry and Remote Sensing, 211, 406–424.

Hassaan M.A., Abdallah S.M., Shalaby E.S.A. and Ibrahim A.A. (2023). Assessing vulnerability of densely populated areas to air pollution using Sentinel-5P imageries: a case study of the Nile Delta, Egypt. Scientific Reports, 13(1). DOI: 10.1038/s41598-023-44186-4

Hou C., Xie Y. and Zhang Z. (2022). An improved convolutional neural network based indoor localization by using Jenks natural breaks algorithm. China Communications, 19(4). DOI: 10.23919/JCC.2022.04.021

Jiang W. (2018). Object-based deep convolutional autoencoders for high-resolution remote sensing image classification. Journal of Applied Remote Sensing, 12(03). DOI: 10.1117/1.jrs.12.035002

Ke C., He S. and Qin Y. (2023). Comparison of natural breaks method and frequency ratio dividing attribute intervals for landslide susceptibility mapping. Bulletin of Engineering Geology and the Environment, 82(10). DOI: 10.1007/s10064-023-03392-0

Li Z., Chen B., Wu S., Su M., Chen J.M. and Xu B. (2024). Deep learning for urban land use category classification: A review and experimental assessment. Remote Sensing of Environment, 311, 114290.

Liu Y., Wang Y., Peng J., Du Y., Liu X., Li S. and Zhang D. (2015). Correlations between urbanization and vegetation degradation across the world's metropolises using DMSP/OLS nighttime light data. Remote Sensing, 7(2), 2067–2088.

Maurya N.K., Pandey P.C., Sarkar S., Kumar R. and Srivastava P.K. (2022). Spatio-Temporal Monitoring of Atmospheric Pollutants Using Earth Observation Sentinel 5PTROPOMI Data: Impact of Stubble Burning a Case Study. ISPRS International Journal of Geo-Information, 11(5). DOI: 10.3390/ijgi11050301

McRoberts R.E., Næsset E., Sannier C., Stehman S. V. and Tomppo E.O. (2020). Remote sensing support for the gain-loss approach for greenhouse gas inventories. In: Remote Sensing, Vol. 12, Issue 11. DOI: 10.3390/rs12111891

Pan Y., Wu J., Liu G., Liu W. and Ma L. (2024). Differential responses of temperature sensitivity of greenhouse gases emission to seasonal variations in plateau riparian zones. Environmental Pollution, 353, 124190.

Pecl G.T., Araújo M.B., Bell J.D., Blanchard J., Bonebrake T.C., Chen I.C., Clark T.D., Colwell R.K., Danielsen F., Evengård B., Falconi L., Ferrier S., Frusher S., Garcia R.A., Griffis R.B., Hobday A.J., Janion-Scheepers C., Jarzyna M.A., Jennings S., . . . Williams S.E. (2017). Biodiversity redistribution under climate change: Impacts on ecosystems and human well-being. In: Science, Vol. 355, Issue 6332. DOI: 10.1126/science.aai9214

Pintelas E., Livieris I.E. and Pintelas P.E. (2021). A convolutional autoencoder topology for classification in high-dimensional noisy image datasets. Sensors, 21(22). DOI: 10.3390/s21227731

Priyadarshini S.L.A., Kaushik V. and Kataria R. (2025). The Role of Anthropogenic Activities, Energy Demand, and Global Climate Change. In: The Intersection of Global Energy Politics and Climate Change: A Comprehensive Analysis of Energy Markets and Economics , 35–61. Springer.

Puspitasari S.A. and Wu C.-F. (2025). Assessing future climate change with a weather generator: A case study in Bali, Indonesia. BIO Web of Conferences, 155, 3003.

Rahaman Z.A., Kafy A. Al, Saha M., Rahim A.A., Almulhim A.I., Rahaman S.N., Fattah M.A., Rahman M.T., S K., Faisal A. Al and Al Rakib A. (2022). Assessing the impacts of vegetation cover loss on surface temperature, urban heat island and carbon emission in Penang city, Malaysia. Building and Environment, 222. DOI: 10.1016/j.buildenv.2022.109335

Rzasa K. and Ciski M. (2021). Determination of the level of sustainable development of the cities - A proposal for a method of classifying Objects based on natural breaks. Acta Scientiarum Polonorum, Administratio Locorum, 20(3). DOI: 10.31648/aspal.6701

Sakti A.D., Anggraini T.S., Ihsan K.T.N., Misra P., Trang N.T.Q., Pradhan B., Wenten I.G., Hadi P.O. and Wikantika K. (2023). Multi-air pollution risk assessment in Southeast Asia region using integrated remote sensing and socio-economic data products. Science of the Total Environment, 854. DOI: 10.1016/j.scitotenv.2022.158825

Saifulloh, M., Sunarta, I. N., Baiquni, M., Trigunasih, N. M., Adikampana, I. M. (2025). Linking annual land subsidence to built-up density across coastal tourism zones via Sentinel-1 differential interferometric synthetic aperture radar. Ecological Engineering & Environmental Technology, 26(9), 325-335.

Scafetta N. (2024). Impacts and risks of "realistic" global warming projections for the 21st century. Geoscience Frontiers, 15(2). DOI: 10.1016/j.qsf.2023.101774

Subramanian V. (2018). Deep Learning with PyTorch: A practical approach to building neural network models using PyTorch. In: O'Reilly Media

Sudarma I., Saifulloh M., Diara I.W. and As-Syakur A. (2024). Carbon Stocks Dynamics of Urban Green Space Ecosystems Using Time-Series Vegetation Indices. Ecological Engineering & Environmental Technology (EEET), 25(9).

Sunarta I.N. and Saifulloh M. (2022a). Coastal tourism: impact for built-up area growth and correlation to vegetation and water indices derived from Sentinel-2 remote sensing imagery. Geojournal of Tourism and Geosites, 41(2). DOI: 10.30892/gtg.41223-857

Sunarta I.N. and Saifulloh M. (2022b). Spatial variation of NO2 levels during the Covid-19 pandemic in the Bali tourism area. Geographia technica, 17(1). DOI: 10.21163/GT_2022.171.11

Sunarta I.N., Suyarto R., Saifulloh M., Wiyanti W., Susila K.D. and Kusumadewi L.G.L. (2022). Surface urban heat island (SUHI) phenomenon in Bali and Lombok tourism areas based on remote sensing. Journal of Southwest Jiaotong University, 57(4). DOI: 10.35741/issn.0258-2724.57.4.44

Susila K.D., Trigunasih N.M. and Saifulloh M. (2024). Monitoring Agricultural Drought in Savanna Ecosystems Using the Vegetation Health Index--Implications of Climate Change. Ecological Engineering & Environmental Technology (EEET), 25(9).

Toersilowati L., Siswanto B., Maryadi E., Susanti I., Suhermat M., Witono A., Sipayung S.B., Rahayu S.A., Aminuddin J. and Lubis R.F. (2022). The Projections of Climate Change using Conformal Cubic Atmospheric Model (CCAM) in Bali-Indonesia. IOP Conference Series: Earth and Environmental Science, 1047(1), 12033.

Trigunasih N.M. and Saifulloh M. (2022). The Investigating Water Infiltration Conditions Caused by Annual Urban Flooding Using Integrated Remote Sensing and Geographic Information Systems. Journal of Environmental Management & Tourism, 13(5), 1467–1480.

Valjarević A., Milanović M., Gultepe I., Filipović D. and Lukić T. (2022). Updated Trewartha climate classification with four climate change scenarios. Geographical Journal, 188(4). DOI: 10.1111/geoj.12458

Wang S., Cohen J.B., Guan L., Lu L., Tiwari P. and Qin K. (2025). Observationally constrained global NOx and CO emissions variability reveals sources which contribute significantly to CO2 emissions. Npj Climate and Atmospheric Science, 8(1), 87.

Xiong X., Liu J., Chen L., Ju W. and Moshary F. (2021). Special issue "remote sensing of greenhouse gases and air pollution." In: Remote Sensing, Vol. 13, Issue 11. DOI: 10.3390/rs13112057

Yang L., Muhammad I., Chi Y.X., Liu Y.X., Wang G.Y., Wang Y. and Zhou X.B. (2022). Straw return and nitrogen fertilization regulate soil greenhouse gas emissions and global warming potential in dual maize cropping system. Science of the Total Environment, 853. DOI: 10.1016/j.scitotenv.2022.158370

Yu Q., Li S. and Chen N. (2024). Urbanization and greenhouse gas emissions from municipal wastewater in coastal provinces of China: Spatiotemporal patterns, driving factors, and mitigation strategies. Environmental Research, 259, 119398.